CFD Letters

Journal homepage:
https://semarakilmu.com.my/journals/index.php/CFD_Letters/index
ISSN: 2180-1363

Numerical Optimization for Aerodynamic Performance of Nose Cone of FSAE Vehicle through CFD

Amol Dhumal[1], Nitin Ambhore[1,*], Pradip Tamkhade[2], Atharv Marne[1], Nihal Mujawar[1]

[1] Department of Mechanical Engineering, Vishwakarma Institute of Information Technology, Pune, 411048, Maharashtra, India
[2] Department of Mechanical Engineering, Marathwada Mitramandal's College of Engineering, Pune 411052, Maharashtra, India

ARTICLE INFO

Article history:
Received 6 November 2023
Received in revised form 8 December 2023
Accepted 10 January 2024
Available online 30 June 2024

Keywords:
Optimization; Aerodynamic; Nose Cone; CFD

ABSTRACT

This paper presents the optimization and aerodynamic performance of a Formula SAE vehicle nose cone. The purpose of the study is to minimize drag while simultaneously enhancing downforce to improve traction and acceleration of the vehicle. Numerous CAD models of the nose cone were developed, taking into account factors such as chassis dimensions, ground clearance, and Formula SAE rulebook constraints. Computational Fluid Dynamics (CFD) analysis is carried out in ANSYS 2021 Fluent module. The fluid domain was created and meshed using tetrahedral cells, and the flow field was predicted using the Realizable k-ε turbulence model. The simulation results revealed essential information including drag and lift coefficients, as well as pressure and velocity contours. An in-depth analysis of lift and drag coefficients guided the optimization of the nose cone design. The study ultimately identified a nose cone design that yielded the most favorable drag coefficient and is found in the range between 0.2-0.3. The study also observed that the down force is increased by 27%. This design proved highly effective in reducing the vehicle's drag and sufficient downforce to enhance acceleration.

1. Introduction

The aerodynamics domain deals with the study of the behavior of air around a moving object or geometry and how it affects performance. Aerodynamics considerations are of utmost importance in motorsports and race car design as well as commercial vehicles including locomotives. The effect of moving body and its performance is studied by Guerrero *et al.,* [1] and Stucki *et al.,* [2]. Borello *et al.,* [3] reported that, as per the laws of viscous and turbulent flow, the friction at the boundary in a flow increases with an increase in speed proportional to the speed square. Thus, for high-speed vehicles, there is a force called drag force which acts in the direction opposite to the direction of motion of the vehicle by Blocken *et al.,* [4]. Therefore, drag force is one of the major setbacks when it comes to achieving high speeds when the vehicle is in motion. The drag force also increases with speed proportional to the speed square. This affects the overall efficiency of a vehicle reported by Nath *et al.,* [5]. Peng [6] used aerodynamic principles in design to impart a pressure force in a vehicle

* *Corresponding author.*
E-mail address: nitin.ambhore@viit.ac.in (Nitin Ambhore)

https://doi.org/10.37934/cfdl.15.11.161171

without increasing the vehicle weight along with drag force reduction. This helps to improve traction and cornering and turning ability at high speed. Gupta [7] concluded that the factors affecting the drag are the density of fluid, the area of contact of geometry with air, and the speed of the vehicle. Oxyzoglou [8] investigated the effect of aerodynamics on the vehicle's performance and behavior. The author concluded that an aerodynamic package produces noticeably more drag at all speeds. Islam *et al.,* [9] investigated the performance of airfoils using 2D CFD. The outcome demonstrates that, due to greater flow velocities, the wing's lift coefficient increases proportionately as the Reynolds number rises. But because of an increase in turbulence, this Reynolds number increase also leads to a higher drag coefficient.

Aerodynamics aims at maintaining minimum contact area and keeping the flow streamlined around the vehicle. The factors affecting the drag are the density of fluid, the area of contact of geometry with air, and the speed of the vehicle. Thus, aerodynamics aims at maintaining minimum contact area and keeping the flow streamlined around the vehicle. The estimation of drag force is given in Eq. (1).

$$F = Cd \times A \times \frac{\rho V^2}{2} \tag{1}$$

Where, Cd= Coefficient of drag, ρ = density of air, V = velocity of air, A = area in contact

The study is based on a standard rulebook similar to the Formula 1 car. There are events held by the Society of Automotive Engineers (SAE) in India and around the world where student teams design and manufacture formula student-style vehicles based on the rulebook and compete in these competitions every year at national and international levels. The aerodynamic properties and handling stability of a race car under various body attitudes were studied by *Zhang et al.,* [10]. The results showed that increasing cornering causes the car's downforce to increase by 11.39%, drag to decrease by 2.85%, and lift-to-drag ratio to increase by 14.70%. According to Fudhail *et al.,* [11], aerodynamic resistance can be greatly decreased by properly arranging vehicles traveling at cruising speed on highways.

Optimization is transforming a real-life problem into a mathematical problem or equation and solving it numerically. The Navier-Stokes equation is considered along with some fundamental questions to understand the aerodynamics with molecules of air in random motion. Houqe *et al.,* [12] presented numerical optimization referring to the method of choosing or selecting the best element abiding by the design parameters and criterion. Kwak *et al.,* [13] investigated different nose shapes and found a reduction in aerodynamic drag.

For analytical validation and design optimization of the nose cone, Computational Fluid Dynamics (CFD) analysis is employed. The CFD analysis involves analytical and numerical analysis of the dynamic behavior of a fluid around a geometry by applying necessary boundary conditions and flow equations. The analysis can be conducted to understand the effect of airflow over geometry using which revisions can be carried out to improve the results.

Nishikawa [14] reported grid optimization in using CFD which refers to the process of refining or adapting the computational mesh or grid used in a CFD simulation to improve the accuracy and efficiency of the simulation. Grid or mesh is a discretization of the physical domain and is an important aspect of the simulation, and the governing equations of fluid flow are solved numerically as reported by Fellows [15]. Lee *et al.,* [16] studied that grid refinement involves adding more grid points or elements in areas where high gradients or complex flow patterns are expected. Adaptive mesh refinement (AMR) is a technique where the grid is dynamically refined during the simulation based on certain criteria which helps in obtaining accurate results according to Asral *et al.,* [17]. Wang *et al.,* [18] reported overall grid optimization and found that critical step in CFD simulations,

as it directly impacts the quality of results and the computational resources required. A well-optimized grid can lead to more accurate and efficient simulations, which are essential for engineering and scientific applications that rely on CFD according to *Wu et al.,* [19]. Bryant and Ng [20] utilized RNG k-ϵ turbulence models to conduct CFD analysis. The model shows good agreement with experimental data. The author suggested the use of the k-ϵ turbulence model to conduct simulation for better accuracy.

The nose is a part whose primary function is to cover the cockpit of the vehicle. The nose cone has to satisfy the rulebook as well. The major ruling for the nose cone is that the edges that can come in contact with pedestrians during an impact should have a 38 mm fillet. Thus any shape that can be developed that can satisfy the mentioned two conditions. For analytical validation and design optimization of the nose cone, CFD analysis is employed. In this paper, the design is created in Solidworks and has been tested iteratively for obtaining drag and downforce (negative lift) values. This ratio is employed as a comparison factor between the current design and the design of the nose of the previous vehicle. The purpose of the study is to minimize drag while simultaneously enhancing downforce to improve traction and acceleration of the vehicle.

2. Methodology

The governing equations of Computational Fluid Dynamics (CFD) describe the fundamental principles that govern the behavior of fluid flow. Conservation equations form the foundation of continuum mechanics and are essential in describing the behavior of physical systems, including fluid dynamics. The generalized 3D continuity equation is given by Eq. (2) and momentum equations are given by Eq. (3), Eq. (4) and Eq. (5).

$$\frac{\partial u}{\partial x} + \frac{\partial v}{\partial y} + \frac{\partial w}{\partial z} = 0 \tag{2}$$

$$u\frac{\partial u}{\partial x} + v\frac{\partial u}{\partial y} + w\frac{\partial u}{\partial z} = -\frac{1}{\rho}\frac{\partial p}{\partial x} + \frac{\partial^2 u}{\partial x^2} + \frac{\partial^2 u}{\partial y^2} + \frac{\partial^2 u}{\partial z^2} \tag{3}$$

$$u\frac{\partial v}{\partial x} + v\frac{\partial v}{\partial y} + w\frac{\partial v}{\partial z} = -\frac{1}{\rho}\frac{\partial p}{\partial y} + \frac{\partial^2 v}{\partial x^2} + \frac{\partial^2 v}{\partial y^2} + \frac{\partial^2 v}{\partial z^2} \tag{4}$$

$$u\frac{\partial w}{\partial x} + v\frac{\partial w}{\partial y} + w\frac{\partial w}{\partial z} = -\frac{1}{\rho}\frac{\partial p}{\partial y} + \frac{\partial^2 w}{\partial x^2} + \frac{\partial^2 w}{\partial y^2} + \frac{\partial^2 w}{\partial z^2} \tag{5}$$

The venturi effect is a phenomenon that occurs when a fluid flows through a pipe and is forced through a narrow section, resulting in a decrease in pressure and an increase in velocity. This effect is mathematically described by the Bernoulli equation and can be observed in both natural phenomena and industrial applications. It is similar to the sensation one experiences when placing a thumb at the end of a garden hose with the water turned on, where the water's velocity increases as it passes through the restricted area. However, it is important to note that the pressure increases over the smaller surface area, but this constriction in the flow ultimately creates a vacuum-like effect within the water. In the field of fluid dynamics, it's a fundamental principle that as a fluid passes through a constriction, its velocity must increase in accordance with the principle of mass continuity. Simultaneously, its static pressure must decrease following the principle of conservation of mechanical energy. Therefore, any increase in kinetic energy that a fluid gains due to its accelerated velocity through a constriction is offset by a decrease in pressure. Using Bernoulli's equation in the

special case of steady, incompressible, inviscid flows along a streamline, the theoretical pressure drop at the constriction is given by given as Eq. (6).

$$P_1 - P_2 = \frac{\rho}{2}\left(u_2^{\,2} - u_1^{\,2}\right) \tag{6}$$

Where ρ the density of the fluid, u1 is the slower fluid velocity where the pipe is wider, and u2 is the faster fluid velocity where the pipe is narrower.

2.1 Nose Cone Shape Selection

The nose cone is one of the largest components and the first component coming in contact with the airflow. Hence it is necessary to optimize the shape for aerodynamic performance. The analytical results can be validated using the efficiency formula which is the ratio of lift coefficient and drag coefficient. The aim was to achieve the lowest drag coefficient for the nose cone design. Thus the iterations were performed and accordingly, the shape was optimized after every iteration until the optimum drag, lift coefficient, and downforce were achieved. The main function of the nose cone is to divert airflow away from the cockpit. Design of nose cone is very important aspect of high speed vehicle according to Moradi *et al.,* [21]. The basic shape of the geometry was created using the chassis CAD model as a reference and keeping in mind the rulebook. It started with the design with the primary aim to cover the whole cockpit. Solidworks software is used for modeling the nose of a vehicle. The initial geometry was created with the dimension constraints of the chassis. The dimensions are a length of 1130 mm, a height of 550 mm, and a maximum width of 500 mm. A major effort was put in to make the bullet shape the conical tip of the geometry and keep the curved shape to maintain a streamlined flow around the geometry. Further, the shape changed as per analysis results and requirements for several iterations before the final shape was determined. Figure 1 shows the iterations for the nose cone design.

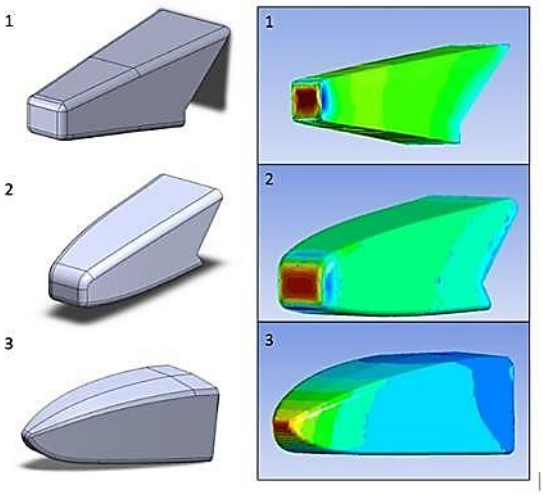

Fig. 1. Nose cone design iterations

2.2 Design Optimization

The various nose designs were optimized by iterative optimization. Figure 2 depicts the step-by-step optimization process, where each iteration involves conducting CFD analysis under the same

boundary conditions. In each iteration, areas with significant drag were pinpointed and subsequently addressed in the following iteration. The visual representation of this iterative improvement process can be found in the flowchart presented in Figure 2. In order to investigate the effects of unsteady vehicle aerodynamics on the vehicle's motion, conventional analysis of the vehicle's motion using quasi-steady aerodynamic forces and one-way coupled analysis with fixed vehicle attitude can also be conducted.

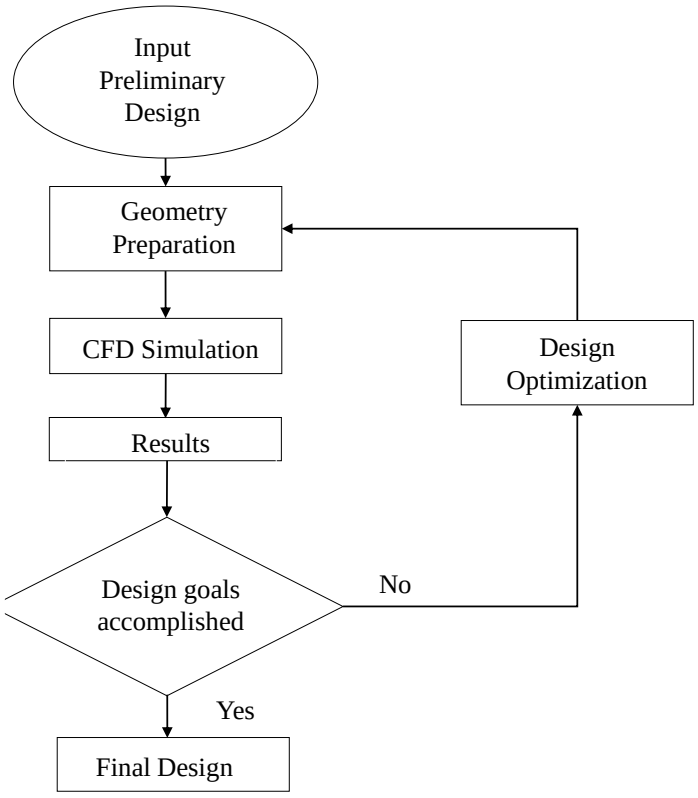

Fig. 2. Optimization Method

2.3 Simulation

The Simulations were performed using the ANSYS Fluent solver package (2021 R2). The characteristic length of the nose was maintained at 1.2 meters. Given a flow velocity of 20 m/s, the resulting characteristic Reynolds Number (Re) is determined to be 1.64 x 10^6 using the Eq. (7).

$$R = \frac{\rho V d}{\mu} \tag{7}$$

These calculations indicate that the airflow around the nose is likely to exhibit turbulent behavior. Consequently, turbulence models were employed for the simulations. Turbulence models are designed to solve the Reynolds-Averaged Navier-Stokes (RANS) equations. Multiple turbulence models aim to solve these RANS equations by making specific assumptions. The assumptions inherent to a particular model lead to a specific set of equations that are derived from the RANS equations based on those assumptions. Turbulence models can range from relatively simple to highly complex. For instance, the SpalartAlmaras model relies on a single equation, the k-epsilon model uses two equations, and the k-omega model employs two equations. The number of equations in a turbulence model directly correlates with the model's complexity and accuracy. More equations

generally result in a more intricate model that offers greater accuracy but demands higher computational resources during simulations hence k-epsilon model is employed for current study and given by Eq. (8).

$$\frac{\partial}{\partial t}(\rho\kappa) + \frac{\partial}{\partial x_i}(\rho k u_i) = \frac{\partial}{\partial x_j}\left[\left(\mu + \frac{\mu_t}{\sigma_k}\right)\left(\frac{\partial k}{\partial x_j}\right)\right] + P_k - \rho\varepsilon + \rho g k \quad (8)$$

2.4 Grid Convergence Analysis

A grid convergence analysis was done on the nose prior to starting the comparison investigation. It is a systematic analysis used to evaluate the accuracy and convergence of numerical solutions by varying the grid resolution as per Edalatpour *et al.,* [22]. This grid convergence study utilized the ANSYS Fluent Package, employing a Double Precision Serial Solver and the k-epsilon turbulence model for all simulations. The process began with meshing the geometry at a coarse level. Subsequently, the simulation results, particularly focusing on the Coefficient of Drag, were monitored using this initial mesh. The mesh refinement process was then systematically applied, gradually increasing the level of mesh fineness. This refinement continued until the results reached a point where further mesh refinement no longer produced significant variations in the outcomes. The final mesh size selected was 20mm as shown in Table 1.

Table 1
Mesh size study

Number of elements	Mesh size	Coefficient of drag
681783	100 mm	0.4284
681783	50 mm	0.3466
3528057	20 mm	0.2956
19201934	10 mm	0.2931

2.5 Post-processing

The analysis was conducted using the Fluid Flow (Fluent) analysis system within the ANSYS Workbench Software Package. During the pre-processing, a Fluid Domain was created around the nose cone. In the case of external aerodynamics, the fluid domain takes on the form of a rectangular box, essentially emulating a virtual wind tunnel. The entrance of the wind tunnel is placed at 1.5m ahead of the geometry and the inlet velocity is defined on it. The exit of the wind tunnel is placed at 2.5m behind the geometry, it acts as a pressure outlet. The side walls of the tunnel are placed 0.5m further from the geometry Multigrid techniques are used to accelerate the convergence of equation RANS.

To establish the total layer height, estimating the thickness of the boundary layer is needed. Utilizing the ANSA Y+ calculator with a characteristic length of 1.2 meters and a velocity of 20 m/s, the initial layer height is estimated to be approximately 5.4 x 10^{-4} m as shown in the figure. Consequently, we proceed to create a total of six layers. The first three layers have a fixed absolute height of 0.5 mm, while the subsequent three layers exhibit a growth factor of 1.2 as shown in Figure 3. The Y+ thickness was calculated using online tools, taking into account parameters such as the Reynolds Number, Flow Velocity, Geometry, and other relevant factors. Table 2 shows Analysis settings summary.

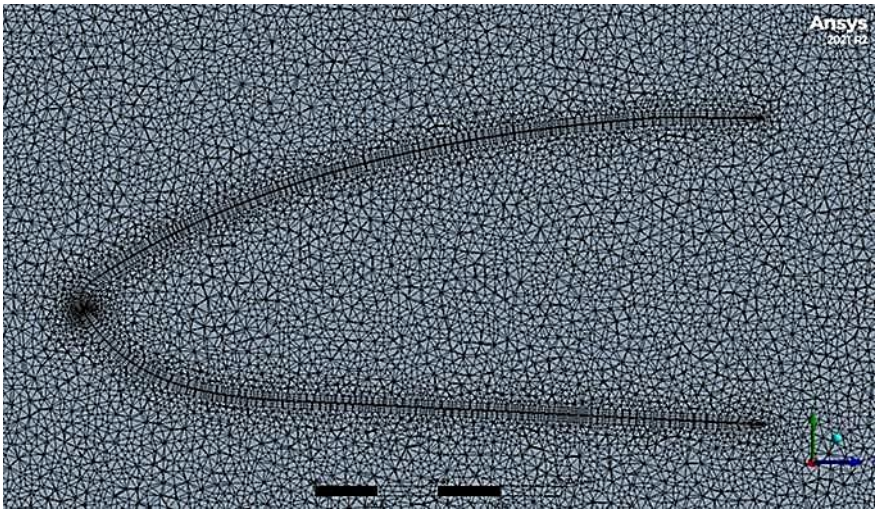

Fig. 3. Final meshing of the nose cone

Table 2
Analysis settings summary

Parameter			**Description**
Mesh details	Method		Tetrahedron
	Element size		20 mm
	Inflation layer	Element Size	0.0005 mm
		No. of layers	6
		Growth ratio	1.2
Setup	Boundary condition	Inlet	Inlet Velocity, 20m/s, Turbulent Intensity 1% and Viscosity ratio 10
		Outlet	Pressure Outlet, Turbulent Intensity 1% and Viscosity ratio 10
		Tunnel walls	Stationary walls, No slip condition
		Road	Moving Wall, 20m/s horizontal translational velocity
Solution	Methods		Coupled Solver with Second Order Upwinded Momentum and Second Order Upwinded Turbulence Kinetic Viscosity
	Initialization		Hybrid Initialization
Drag coefficient on the Nose surface Monitors.			
			Lift coefficient on the Nose surface

3. Results and Discussions

The comparative study aimed to optimize the drag coefficient as the primary parameter of interest. Since the simulations were exclusively conducted on the 2D nose profile and not on the complete 3D assembled CAD model of the car, the absolute drag values obtained lack meaningful context. Nonetheless, it effectively assesses the relative performance of the various nose cones in terms of drag reduction by considering the relative values of the drag coefficients. Table 3 shows the drag coefficient and drag coefficient for the first three iterations.

Table 3
Comparison of drag coefficient and drag coefficient

Iteration	Drag coefficient (Cd)	Drag force (Cl)
1	0.4684	27.51 N
2	0.3847	18.83 N
3	0.2834	11.57 N

The outcomes of the comparative study indicated that Iteration 3 is the most suitable for the intended purpose. Consequently, this particular geometry is selected, and additional research into the flow patterns around this geometry is conducted to fine-tune its shape for drag reduction. Interestingly, this profile also exhibited the lowest amount of lift, making it the most downforce-generating geometry. The subsequent stage of the design process entailed the observation of fluid flow patterns across different contour configurations like pressure, velocity distribution, etc.

Figure 4 shows the convergence for the drag coefficient. It is revealed that the drag coefficient for nose1 does not change substantially after 40 iterations and is found as 0.4684. Figure 5 shows the convergence for the lift coefficient. It is revealed that the lift coefficient for nose1 does not change substantially after 20 iterations and is found as 1.2.

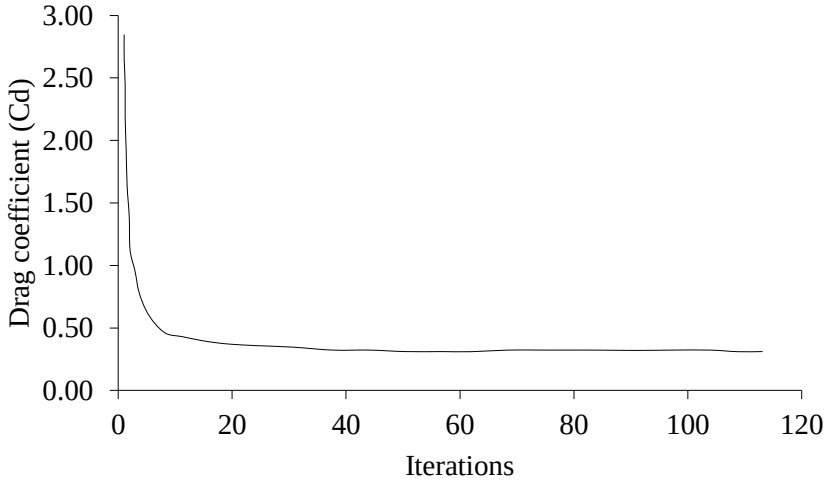

Fig. 4. Convergence for Cd of selected nose cone

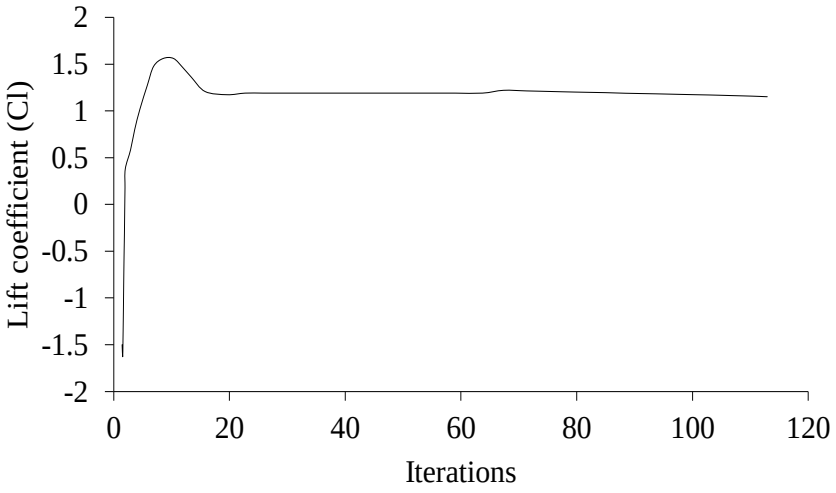

Fig. 5. Convergence for Cl of selected nose cone

The velocity contour in Figure 6 illustrates the variation in airflow velocity between the upstream and downstream sections. Eq. (5), which represents the continuity equation, defines the connection between fluid area and velocity. It is crucial to note that as per the law of conservation of mass, the airflow velocity, specifically air in this context, should be higher in the lower portion of the nose surface to reduce pressure in that area. In Figure 6 the red-colored region signifies an increase in velocity below the lower section of the nose, in comparison to the flow velocity over the nose. Within this red coloured region, the highest velocity observed in the flow field is recorded as 24.87 meters per second. This maximum velocity value indicates the peak speed in that particular area of increased flow velocity below the lower section of the nose. The information provided in the description of Figure 6 suggests that there is a region beneath the nose of some object where the flow velocity increases notably compared to the flow velocity observed directly over the nose. This observation of increased velocity, highlighted in red, indicates a specific flow pattern or phenomenon occurring in that area of the flow field.

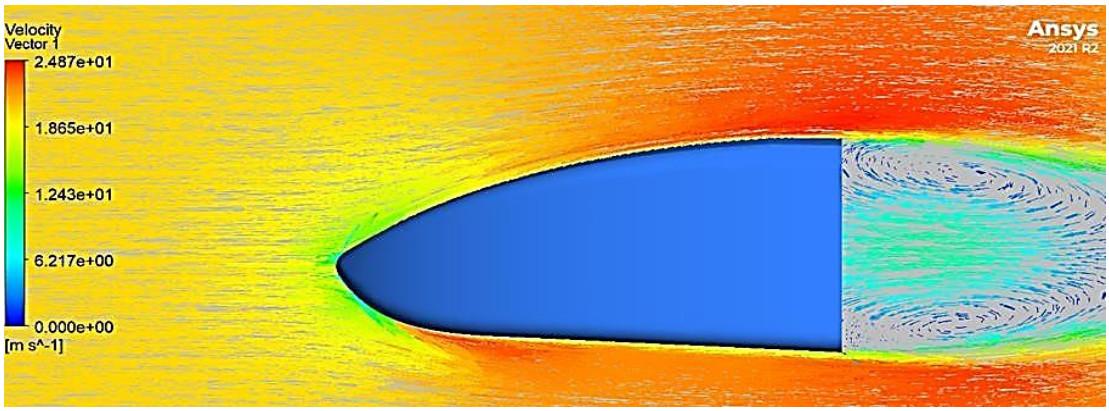

Fig. 6. Velocity contour

Figure 7 represents a visualization, such as a pressure contour plot, illustrating the pressure distribution around an object in a flow field. The pressure contour displays a notable contrast in pressure between the upper and lower boundary layers of the surface. Following the stagnation of air at the boundary layer near the tip of the nose, the airflow divides, spreading in both the upstream and downstream directions. The airflow moves with high velocity at the lower portion of the nose as seen in Figure 7, ultimately decreasing the air pressure in that certain area. The airflow at the upper portion of the nose is found as very high. The pressure difference of 420 Pa is generated which creates strong downforce.

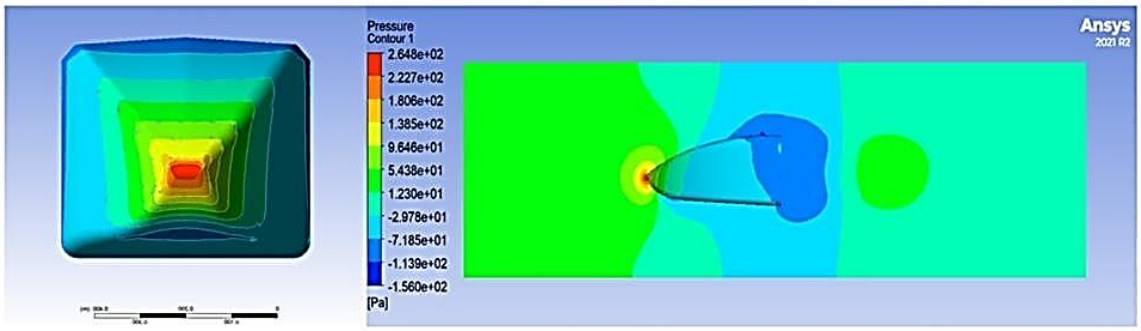

Fig. 7. Pressure contour

Figure 8 depicts a velocity vector representation of the flow field around an object. The velocity vector representation indicates that there is an attached flow characterized by high stability around the nose. This stability is a direct consequence of the streamlined shape of the body. This is needed to designed and promote smooth and stable airflow, minimizing turbulence and enhancing aerodynamic performance. The maximum velocity is observed as 24.06 m/s. This is observed in the flow field and object's streamlined shape.

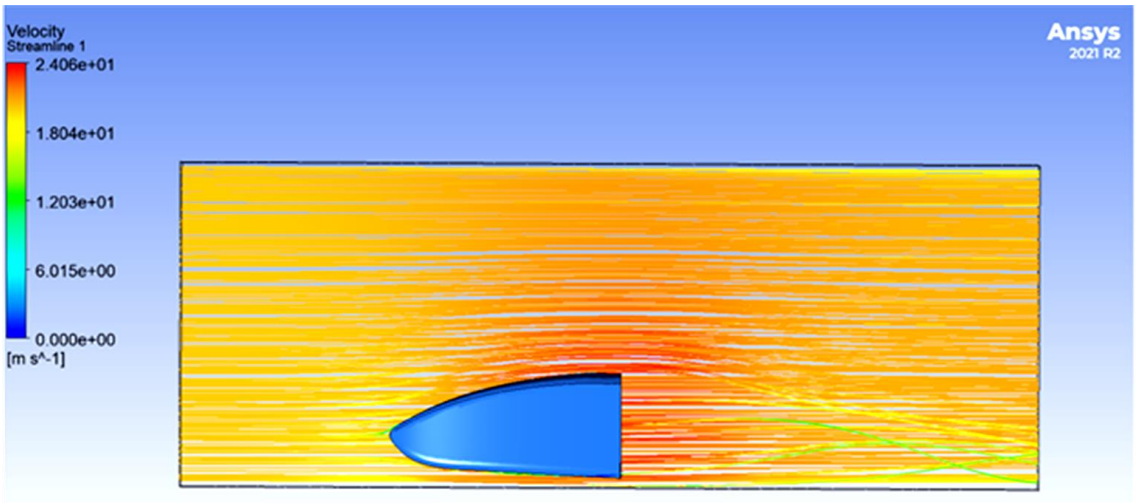

Fig. 8. Velocity vector contour

4. Conclusion

Numerical optimization for the aerodynamic performance of the nose cone of the FSAE vehicle is presented. The drag coefficient and lift coefficient have been studied using CFD simulation by varying element sizes. The drag coefficient for an element size of 100 mm is found as 0.4684 and for an element size of 10 mm, it is observed as 0.2931. The drag coefficient for an element size of 20 mm is observed as 0.2956. It is concluded that the drag coefficient for element sizes of 20 mm and 10 mm gives almost similar results. Hence, it is recommended to use a 20 mm element size to save computational time and memory and obtain the optimum results. For the aerodynamic effect, a significant reduction in the drag force of the geometry is observed. For nose shape 1, the drag force is observed as 27.51 N, and corresponding the coefficient is observed as 0.4684, which has reduced to around 18.83 N for a drag coefficient of 0.3847. For nose shape 3, the drag force has dropped significantly to 11.57 N with a drag coefficient is 0.2834. The velocity and pressure contours give an idea about how the effect of shape change and addition of curvature has contributed to the reduction of drag and also pointed shape of the tip affected reducing the stagnation point at the tip of the nose cone.

Acknowledgment

This research was not funded by any grant.

References

[1] Guerrero, Alex, Robert Castilla, and Giorgio Eid. "A numerical aerodynamic analysis on the effect of rear underbody diffusers on road cars." *Applied Sciences* 12, no. 8 (2022): 3763. https://doi.org/10.3390/app12083763

[2] Stucki, Chad L., and Daniel Maynes. "Drag reducing nose fairings for existing freight train locomotives." *Advances in Aerodynamics* 4, no. 1 (2022): 37. https://doi.org/10.1186/s42774-022-00131-z

[3] Borello, G., S. Beccio, S. Limone, G. Ferro, P. Bergamini, and F. B. Quagliotti. *The role of the moving ground for automotive wind tunnel testing on race cars*. No. 1999-01-0647. SAE Technical Paper, 1999. https://doi.org/10.4271/1999-01-0647

[4] Blocken, Bert, and Yasin Toparlar. "A following car influences cyclist drag: CFD simulations and wind tunnel measurements." *Journal of Wind Engineering and Industrial Aerodynamics* 145 (2015): 178-186. https://doi.org/10.1016/j.jweia.2015.06.015

[5] Nath, Devang S., Prashant Chandra Pujari, Amit Jain, and Vikas Rastogi. "Drag reduction by application of aerodynamic devices in a race car." *Advances in Aerodynamics* 3 (2021): 1-20. https://doi.org/10.1186/s42774-020-00054-7

[6] Peng, Haibing. "A method for evaluation of aerodynamic lift and drag based on statistical mechanics." *Physics of Fluids* 35, no. 5 (2023). https://doi.org/10.1063/5.0146386

[7] Gupta, A. (2018). Cost Effective Manufacturing and Optimization of the Formula Student Nose Cone, IRJET.

[8] Oxyzoglou, Ioannis. "Design & development of an aerodynamic package for a FSAE race car." *University Of Thessaly, pág* 38 (2017).

[9] Islam, Md Saifi Bin, Muhammad Faiz Ahmed, and Abdullah Al Saad. "Numerical Investigation on the Aerodynamic Characteristics of a Wing for Various Flow and Geometrical Parameters." *Malaysian Journal on Composites Science and Manufacturing* 12, no. 1 (2023): 13-30. https://doi.org/10.37934/mjcsm.12.1.1330.

[10] Zhang, Zhe, Qiang Wang, Shida Song, Chengchun Zhang, Luquan Ren, and Yingchao Zhang. "Joint research on aerodynamic characteristics and handling stability of racing car under different body attitudes." *Energies* 15, no. 1 (2022): 393. https://doi.org/10.3390/en15010393

[11] Munir, Fudhail Abdul, Muhammad Najhi Fauzi, and Ridhwan Jumaidin. "Numerical Study of The Effects of Vehicle Arrangement on Aerodynamics Resistance." *Journal of Advanced Research in Fluid Mechanics and Thermal Sciences* 98, no. 1 (2022): 67-72. https://doi.org/10.37934/arfmts.98.1.6772.

[12] Hoque, Md Araful, Md Saifur Rahman, Khairun Nasrin Rimi, Abdur Rahman Alif, and Mohammad Rejaul Haque. "Enhancing formula student car performance: Nose shape optimization via adjoint method." *Results in Engineering* 20 (2023): 101636. https://doi.org/10.1016/j.rineng.2023.101636

[13] Kwak, Minho, Suhwan Yun, Yeongbin Lee, Hyeokbin Kwon, Kyuhong Kim, and Dong-Ho Lee. "Optimum nose shape of a front-rear symmetric train for the reduction of the total aerodynamic drag." *Journal of Mechanical Science and Technology* 27 (2013): 3733-3743. https://doi.org/10.1007/s12206-013-0918-9

[14] Nishikawa, Hiroaki. "Beyond interface gradient: a general principle for constructing diffusion schemes." In *40th fluid dynamics conference and exhibit*, p. 5093. 2010. https://doi.org/10.2514/6.2010-5093

[15] Fellows, Neil A. "Experimental modeling of a formula student carbon composite nose cone." *Materials* 10, no. 6 (2017): 620. https://doi.org/10.3390/ma10060620

[16] Lee, Minhyung, Gwanyong Park, Changyoung Park, and Changmin Kim. "Improvement of grid independence test for computational fluid dynamics model of building based on grid resolution." *Advances in Civil Engineering* 2020 (2020): 1-11. https://doi.org/10.1155/2020/8827936

[17] Anuar, Kaspul, and Agung Soegihin. "Aerodynamic Analysis of Unnamed Aerial Vehicle Serindit V-2 Using Computational Fluid Dynamics." *Journal of Advanced Research in Fluid Mechanics and Thermal Sciences* 93, no. 1 (2022): 83-93. https://doi.org/10.37934/arfmts.93.1.8393.

[18] Wang, Shuguang, and Yonghwan Kim. "Adaptive grid deformation method for CFD application to hull optimization." In *IOP Conference Series: Materials Science and Engineering*, vol. 1288, no. 1, p. 012043. IOP Publishing, 2023. http://doi.org/10.1088/1757-899X/1288/1/012043

[19] Wu, Zhengren, Shuguang Li, Mei Liu, Songling Wang, Hongyue Yang, and Xiujun Liang. "Numerical research on the turbulent drag reduction mechanism of a transverse groove structure on an airfoil blade." *Engineering Applications of Computational Fluid Mechanics* 13, no. 1 (2019): 1024-1035. https://doi.org/10.1080/19942060.2019.1665101

[20] Bryant, Daniel John Ebrahim, and K. C. Ng. "Numerical modelling of hydraulic jump using mesh-based cfd method and its comparison with lagrangian moving-grid approach." *Journal of Advanced Research in Micro and Nano Engineering* 10, no. 1 (2022): 1-6.

[21] Moradi, R., M. Mosavat, M. Barzegar Gerdroodbary, A. Abdollahi, and Younes Amini. "The influence of coolant jet direction on heat reduction on the nose cone with Aerodome at supersonic flow." *Acta astronautica* 151 (2018): 487-493. https://doi.org/10.1016/j.actaastro.2018.06.026

[22] Edalatpour, Amirhossein, A. Hassanvand, M. Barzegar Gerdroodbary, Rasoul Moradi, and Y. Amini. "Injection of multi hydrogen jets within cavity flameholder at supersonic flow." *International Journal of Hydrogen Energy* 44, no. 26 (2019): 13923-13931. https://doi.org/10.1016/j.ijhydene.2019.03.117